A MULTI-SCALE DYNAMIC NETWORK SIMULATOR USED AS A MEANS TO QUANTIFY HETEROGENEITIES OF PERMEABILITY AND WETTABILITY IN POROUS MEDIA

Christos D. Tsakiroglou , Christos Aggelopoulos, Varvara Sygouni
Foundation for Research and Technology Hellas- Institute of Chemical Engineering and High Temperature Chemical Processes, Stadiou str., Platani, P.O.Box 1414, 26504 Patras, Greece

This paper was prepared for presentation at the International Symposium of the Society of Core Analysts held in Abu Dhabi, UAE 29 October-2 November, 2008

ABSTRACT

A hierarchical, network-type, dynamic simulator of the immiscible displacement in heterogeneous porous media is developed to simulate the rate-controlled displacement of two fluids at two scales, from the pore network to the core scale. A cubic network is constructed, where each node is assigned a permeability which is chosen randomly from a distribution function. Moreover, heterogeneities in wettability can be entered as randomly or non-randomly distributed contact angles. The degree of heterogeneity is quantified by the width of the distribution function of the corresponding property (permeability, contact angle). The capillary pressure at each node is calculated by combining a generalized Leverett J-function with a Corey type model. The simulator is used to examine the sensitivity of the transient responses of the axial distribution of fluid saturation and total pressure drop across the network to the heterogeneity as expressed by the permeability / wettability distribution functions, and the capillary number. Moreover the effects of heterogeneity on the overall (up-scaled) relative permeability functions are elucidated. Input parameters are obtained from either quasi-static simulations of pressure-controlled immiscible displacement in pore networks, or inverse modeling of flow tests on heterogeneous soil columns with the aid a multi-flow path model.

INTRODUCTION

Microscopic pore structure analysis (Tsakiroglou and Ioannidis, 2008) along with the immiscible and miscible displacement experiments performed on undisturbed soil columns (Aggelopoulos and Tsakiroglou, 2005, 2007a,b, 2008) revealed that the microporous matrix of this soil (mixture of sand, clay and silt) is heterogeneous at multiple scales, and flow regime is dominated by preferential paths. The capillary pressure and relative permeability curves at a mesoscopic scale (1-2 cm) can be produced by either inverse modeling of the datasets of immiscible displacement experiments (Aggelopoulos and Tsakiroglou, 2007b, 2008) or quasi-static simulation of the two-phase flow in pore-and-throat networks (Tsakiroglou, 2006). Given that the size of the grid utilized by

macroscopic two-phase flow simulators is much larger than 1 cm, whereas viscous and gravity effects become pronounced at large distances, we need computational tools to incorporate higher scale heterogeneities into the up-scaled relative permeability curves. Moreover, flow tests on soil columns (Aggelopoulos and Tsakiroglou, 2005, 2006) and wavelet analysis of the pressure drop signals measured during immiscible displacement experiments on fractional-wet model porous media (Sygouni et al., 2006, 2007b) have revealed that heterogeneities in permeability or wettability are reflected in the transient responses of the variables measured during core-scale tests (pressured drop, water saturation). From macroscopic numerical simulations in heterogeneous porous media (Ataie-Ashtiani et al., 2002; Das et al., 2004), and up-scaling procedures (Braun et al., 2005) it has become evident that the macro-scale heterogeneities affect strongly the transient flow pattern and the shape of the up-scaled capillary pressure and relative permeability curves. In the following, a large-scale network type dynamic simulator of the downward and rate-controlled displacement of one fluid by another is developed to (i) identify and quantify eventual large-scale heterogeneities of natural porous media (soils, rocks), and (ii) determine the overall (up-scaled) relative permeability curves.

LARGE-SCALE SIMULATION

The basic components of the hierarchical dynamic simulator of immiscible displacement in heterogeneous porous media is illustrated in Fig.1. A node can be regarded as a single or dual pore-and-throat network of a given overall permeability. The $P_c(S_w), k_{rw}(S_w), k_{ro}(S_w)$ functions of this node can be determined by simulating oil/water drainage in such a network by tracking the quasi-static (Tsakiroglou, 2006) or dynamic (Gharbi and Blunt, 2005) motion of menisci during pressure-controlled or rate-controlled flow tests. Depending on the selected size of elementary units (nodes), a cubic network is so constructed that each node is assigned a constant permeability which is chosen randomly from a log-normal distribution function of macro-heterogeneity, $\langle k \rangle, \sigma_{k^*}$. The local relative permeability functions, $k_{rw}(S_w), k_{ro}(S_w)$ and capillary pressure curve, $P_c(S_w)$, of nodes (regarded as homogenized blocks) may be set equal either to the ones estimated by inverting rate-controlled displacement experiments by using the multi-flow path model (Aggelopoulos and Tsakiroglou, 2007b), or the ones calculated by simulating the pressure-controlled quasi-static displacement in a pore-and-throat network (Tsakiroglou, 2006)

The rate-controlled displacement of water by oil is simulated by computing the fluid saturation and pressure at each node and taking into account capillary, viscous and gravity forces. The steps of the numerical algorithm are described below.

1. Assignment of permeabilities to nodes (cubes in the right hand side of Fig.1) according to the density distribution function ($\langle k \rangle, \sigma_{k^*}, k^* = k/\langle k \rangle$). The overall permeability is calculated by imposing pressure differences across the network, determining the influx rate with numerical solution of mass balances at nodes, and fitting the results to Darcy law.
1. Calculation of the capillary pressure at each node from its permeability by combining the generalized Leverett J-function with a Corey type model:

$$P_{co}(k) = c\gamma_{ow}\cos\theta\, k^{-\delta} \qquad P_c(k, S_w) = P_{co}(k)\left(\frac{S_w - S_{wi}}{1 - S_{wi}}\right)^{m_c} \tag{1}$$

where γ_{ow} is the oil/water interfacial tension, θ is the contact angle, c, δ, m_c are parameters, P_{co} is the node entry pressure, and S_{wi} is the irreducible water saturation.

2. The input relative permeability functions $k_{rw}(S_w), k_{ro}(S_w)$ are identical for each node (a cube in the left hand side of Fig.1), and can be obtained either with inverse modeling of transient displacemnet tests (Aggelopoulos and Tsakiroglou, 2007b) or pore network simulators of drainage (Tsakiroglou, 2006; Table 1).
3. Gravity can be incorporated into the local capillary pressure by defining the piezometric capillary pressure:

$$P_c'(k, S_w) = P_c(k, S_w) + (\rho_w - \rho_o)gh \tag{2}$$

where ρ_w, ρ_o are the water and oil density, respectively, and h the vertical position of the interface with respect to a reference level.

4. The 2-phase flow Darcy law and current values of fluid saturation are used to calculate the effective conductivity of each node.
5. Each unit cell consists of the $1/6^{th}$ of two adjacent nodes; mass balances of the flow rates in the unit cells adjoining to each node result in a system of coupled linear equations the solution of which provides the pressure field.
6. The current flow rates of the invading fluid are utilized to calculate the time spans required for the partial filling ($1/10^{th}$ -$1/5^{th}$) of each unit cell with oil. The calculations of time are restricted to unit cells where oil and water coexist and no entrapment of water has taken place. Afterwards the minimum time span is determined.
7. The distribution of fluid saturation at each node is updated according to the minimum time span and current flow rates.
8. The up-scaled oil and water relative permeability functions of the network (network of cubes in the right hand-side of Fig.1) are calculated. A constant pressure difference is imposed across the large-scale network, mass balances are applied to each node, the system of coupled linear equations is solved and the overall oil and water outflow rates along with the pressure difference are introduced into the two-phase flow Darcy equations.
9. The pressure difference across the large-scale network is so adjusted that the overall oil influx rate agrees with the input superficial velocity. The overall influx flow rate, Q_{oil}, of the injected fluid (oil) is calculated for various values of the pressure difference, ΔP, imposed across the network, by solving the system of coupled linear equations. The results are fitted to the linear relationship:

$$\Delta P = AQ_{oil} + B \tag{3}$$

so that the parameters A, B are estimated.

10. The procedure is repeated from step (5) and on, until no change of saturation and total pressure drop occur.

SENSITIVITY ANALYSIS AND LARGE-SCALE PROPERTIES

Simulated responses of water saturation profile & pressure drop

The quasi-static pressure-controlled oil (n-dodecane)/ NaCl aqueous solution drainage was simulated, under various values of the contact angle, in a cubic pore-and-throat network (Tsakiroglou, 2006) where the statistics of pore- and throat- diameter distributions was comparable to that of the micro-porosity of soil samples collected from a site contaminated with jet fuel (soil sample C7, Tsakiroglou and Ioannidis, 2008). The small-scale simulated capillary pressure and relative permeability curves were fitted with the Leverett and Corey type equations to estimate the input parameters for the large-scale simulator (Table 1). A network with the dimensions 10x5x5 nodes (10cmx5cmx5cm) and $\langle k \rangle$=50mD was constructed and the large-scale simulator was used to examine the effects of the standard deviation of the local (node) permeability distribution on the transient responses of the axial saturation profile and total pressure drop when the displacement is performed under constant flow rate (Fig.2a-d). The capillary number, defined by

$$Ca = \frac{\mu_o u_0}{\gamma_{ow}} \tag{3}$$

was $Ca = 1\text{x}10^{-7}$, where $\mu_o = 0.00135$ Pa s, $\mu_w = 0.001$ Pa s, $\gamma_{ow} = 50\text{x}10^{-3}$ N m^{-1}.Both the fluid saturation profile (Fig.2a-c), and the total pressure drop across the entire porous medium (Fig.2d) are sensitive to the variability of node permeability distribution.

The sensitivity of the water saturation profile and pressure drop to capillary number $Ca = \mu_o u_o / \gamma_{ow}$ is shown in Fig.3. It seems that as Ca increases, the favourable viscosity ratio, $\kappa = \mu_o / \mu_w = 1.35$, stabilizes the displacement by reducing the front thickness and leading to lower irreducible water saturation (Fig.3a-c). On the other hand, the pressure drop increases substantially because of the pronounced effect of viscous forces on the hydrodynamic terms of the pressure drop at the length scale of the porous medium (~10 cm).

The spatial variation of the capillary pressure over the network nodes may be due not only to heterogeneities of the permeability, but also to heterogeneous wettability. Attempting to simulate conditions of fractional macro-heterogeneity, a large network composed of nodes of identical permeability $k = \langle k \rangle = 50$mD was considered. Each node was assigned randomly a contact angle according to a uniform distribution $[\theta_{min}, \theta_{max}]$. The contact angle distributions were so chosen that the mean contact angle remained constant, $\langle \theta \rangle = 42.5^o$. No significant changes are observed on either the axial saturation profile (Fig.4a-c) or pressure drop response (Fig.4d), although the comparative analysis of oscillating signals (Fig.4d) is not straightforward.

Rate-controlled visualization experiments of immiscible displacement performed on model porous media of controlled fractional wettability revealed that the measured pressure drop relates to the spatial distribution of wettability. The oscillating transient signal of the pressure drop measured across the porous medium was analyzed with multilevel wavelets to produce the best level wavelet details defined as the "best level capillary pressure spectrum" (BLCPS) by minimizing the "entropy" of wavelet approximation (Sygouni et al., 2007). It was found that the displacement growth pattern was reflected in the "energy" of the BLCPS which was correlated explicitly with parameters quantifying the spatial variation of wettability over the porous medium. The same method of multilevel wavelets was used here to analyze the signals of the pressure drop (Figs.2d, 4d) obtained with the dynamic simulation of displacement in large-scale networks (Fig.5a,b).

As the width of the node permeability distribution over the entire network increases, both the mean value, $\langle k_I^* \rangle$, and standard deviation, σ_I^* of the permeability distribution of the oil-occupied nodes increase (Fig.6a,b). On the one hand, the oil is offered the opportunity to move through gradually more permeable paths (Fig.6a). On the other hand, the enhanced variety of node permeabilities (Fig.6b) implies high amplitude pressure drop fluctuations associated with the high frequency in the variation of the capillary pressure. The "facilitation" in oil motion is reflected in the lower energy of the "best level pressure drop spectrum" (BLPDS, Fig.5a). The higher amplitude fluctuations are reflected in higher energy of the BLPDS, especially at advanced times when steady-state conditions are established (Fig.5a). Likewise, as the width of the node contact angle distribution over the entire network increases, the mean value, $\langle P_{ci} \rangle$ of the capillary pressure distribution of the oil-occupied nodes decrease (Fig.6c) while the standard deviation, σ_{pci}, increase (Fig.6d). As it was mentioned earlier, the BLPDS energy has the tendency to decrease with the $\langle P_{ci} \rangle$ decreasing and increase with the σ_{pci} increasing. In this manner, no clear trend appears in BLPDS energy with respect to the width of the contact angle distribution (Fig.5b).

Overall (up-scaled) water and oil relative permeability curves

The up-scaled relative permeability curves were determined by using the foregoing dynamic simulator for large scale networks of dimensions 10x5x5 (node size=1cm) which represent cubic soil elements of volume 250 cm^3. At each time step, and after the fluid distribution in each node has been established, a pressure difference is imposed across each phase and its hydraulic conductivity is calculated by formulating mass balances at nodes and solving numerically the system of coupled linear equations. The effects of the variability of node permeability and contact angle distribution on up-scaled relative permeability curves are shown in Fig.7a and Fig.7b respectively. As the variability of the local permeability is enhanced, both the oil and water relative permeability functions shift to higher water saturations, the displacement is completed much faster, and the residual overall water saturation increases (Fig.7a). As the width of the contact angle range is reduced, both the oil and water relative permeability functions decrease weakly (Fig.7b).
At increasing Ca values, the up-scaled relative permeability curves spread over a wider range of water saturations with the end oil relative permeability increasing (Fig.8).

It seems that oil relative permeability is more sensitive to Ca compared to water relative permeability (Fig.8). The water hydraulic conductivity is associated mainly with the amount of water bypassed during the displacement and remaining in the less-permeable regions of the network. This amount of water is governed by the distribution of heterogeneity and is affected weakly by the rate of displacement.

CONCLUSIONS

A large-scale network-type dynamic simulator was developed to reproduce the transient responses of the pressure drop and axial saturation profile commonly measured across the porous medium in core analysis tests. The simulator may be fed with input parameters resulting either from pore-network simulations or inverse modeling of flow tests on cores, and it seems very promising for the interpretation of large-scale heterogeneities of porous media.

ACKNOWLEDGEMENTS

This work was supported by European Commission, in the course of 6th Framework Program, Subprogram: "Global Change and Ecosystems", contract number: SSPI-CT-2003-004017-STRESOIL.

REFERENCES

1. Aggelopoulos, C.A., and C.D. Tsakiroglou, "Simultaneous determination of the two-phase flow and hydrodynamic dispersion coefficients of soils from transient immiscible and micible displacement experiments", *Proceed. of the 2005 International Symposium of the Society of Core Analysts,* Paper SCA2005-58, Toronto, Canada, August 21-25, 2005.
2. Aggelopoulos, C.A., and C.D. Tsakiroglou, "The longitudinal dispersion coefficient of soils as related to the variability of local permeability", *Water, Air and Soil Pollution* (2007a) **185,** 223-237.
3. Aggelopoulos, C.A., and C.D. Tsakiroglou, **"**From a multi-region model to a multi-flow path model: interpretation of flow tests on heterogeneous cores", *Proceed. of the 2007 International Symposium of the Society of Core Analysts,* Paper SCA2007-43, Calgary, Canada, Sept.9-14, 2007b.
4. Aggelopoulos, C.A., and C.D. Tsakiroglou, "Quantifying the Soil Heterogeneity from Solute Dispersion Experiments", *Geoderma* (2008) **in press**.
5. Al-Gharbi, M.S., and M. Blunt, "Dynamic network modeling of two-phase drainage in porous media", Phys. Rev. E (2005) 71, 016308.
6. Ataie-Ashtiani, B., S.M. Hassanizadeh, M. Oostrom, M. Celia, M.D. White, "Effective parameters for two-phase flow in a porous medium with periodic heterogeneities", *J. Contam. Hydrol.* (2002) **49,** 87-109.
7. Braun, C., R. Helmig, S. Manthey, "Macro-scale effective constitutive relationships for two-phase flow processes in heterogeneous porous media with emphasis on the relative permeability-saturation relationship" *J. Contam. Hydrol.* (2005) **76,** 47-85.
8. Das, D.B., S.M. Hassanizadeh, B.R. Rotter, B. Ataie-Ashtiani, "A numerical study of micro-heterogeneity effects on upscaled properties of two-phase flow in porous media" *Transp. Porous Media* (2004) **56**, 329-350.
9. Sygouni, V., C.D. Tsakiroglou, and A.C. Payatakes, "Capillary pressure spectrometry: toward a new method for the measurement of the fractional wettability of porous media", *Phys. Fluids* (2006) **18**, 053302 (2006).
10. Sygouni, V., C.D. Tsakiroglou, and A.C. Payatakes, "Using wavelets to characterize the wettability of porous materials", *Phys. Rev. E* (2007) **76,** 056304.
11. Tsakiroglou, C.D., "A pore network model to calculate the capillary pressure and relative permeability curves of intermediate-wet reservoirs", *Proceed. of the 2006 International Symposium of the Society of Core Analysts,* Paper SCA2006-45, Trondheim, Norway, Sept. 12-16, 2006.
12. Tsakiroglou, C.D. and M.A. Ioannidis, "Dual porosity modeling of the pore structure and transport properties of a contaminated soil", *Eur. J. Soil Sci.* (2008) **59**, 744-761.

Table 1. Capillary pressure and relative permeability curves from network simulation

$P_c(k) = c\gamma_{ow} \cos\theta\, k^{-\delta}$	$c = 1.6\text{x}10^{-4}$ $\gamma_{ow} = 50\text{x}10^{-3}\ \text{Nm}^{-1}$ $\theta = 6^{o}$ $\delta = 0.738$
$k_{rw} = a\left(\frac{S_w - S_{wi}}{1 - S_{wi}}\right)^{m_{w1}} + (1-a)\left(\frac{S_w - S_{wi}}{1 - S_{wi}}\right)^{m_{w2}}$	$a = 0.155$ $m_{w1} = 0.817$ $m_{w2} = 4.197$ $S_{wi} = 0.21$
$k_{ro} = k_{ro}^{0}\left(\frac{1 - S_w}{1 - S_{wi}}\right)^{m_o}$	$k_{ro}^{0} = 0.737$ $m_o = 2.378$

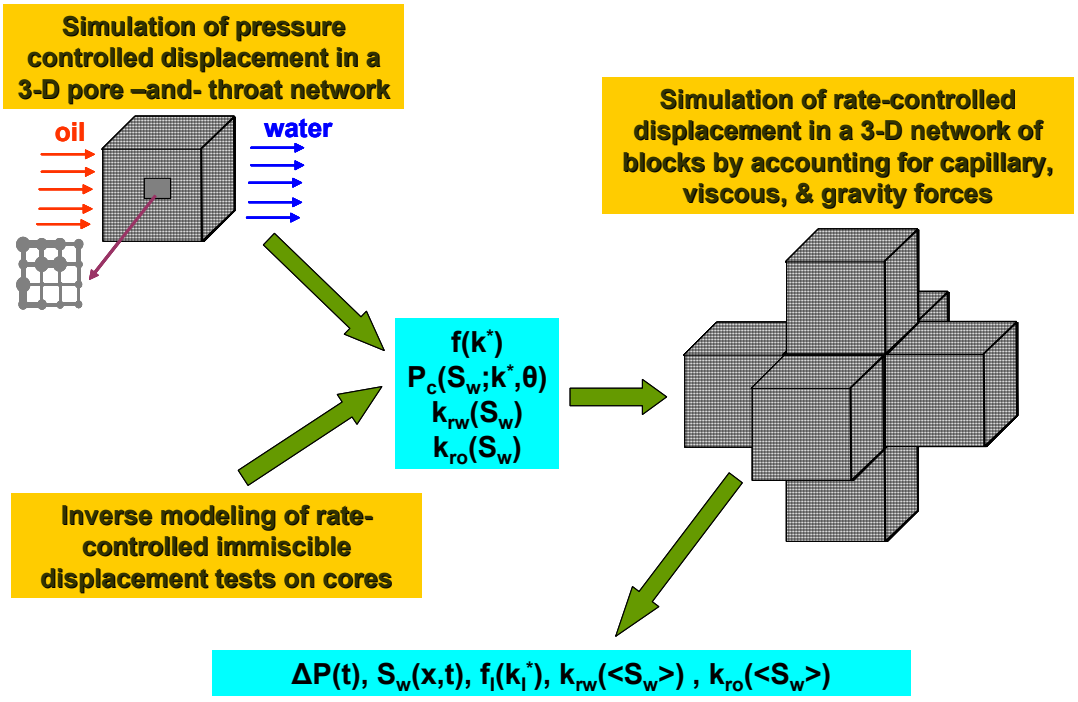

Figure 1. Hierarchical dynamic simulator of immiscible displacement in heterogeneous media.

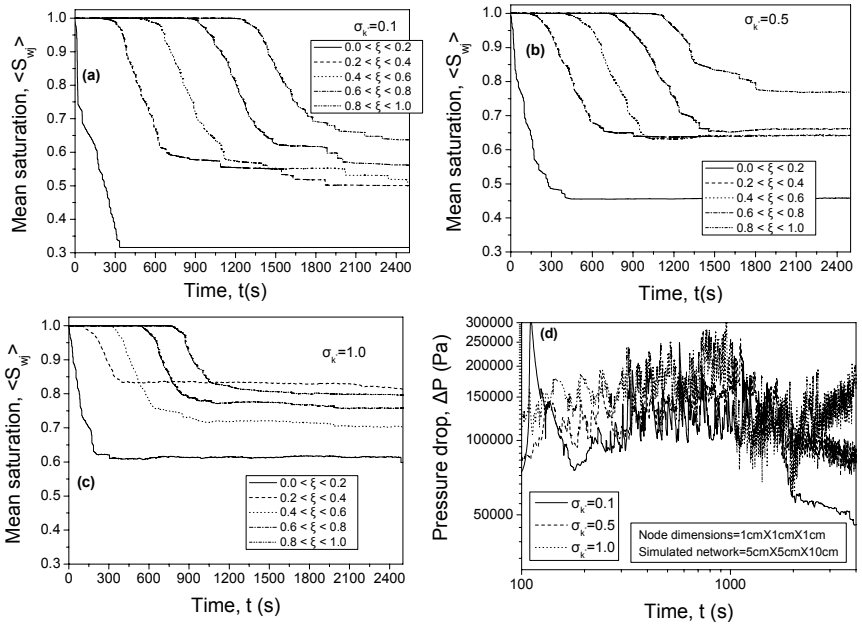

Figure 2. Simulated transient responses of the (a-c) averaged water saturation profiles and (d) pressure drop (node dimensions=1cmX1cmX1cm) for various macro-permeability distributions and parameters of Table 1.

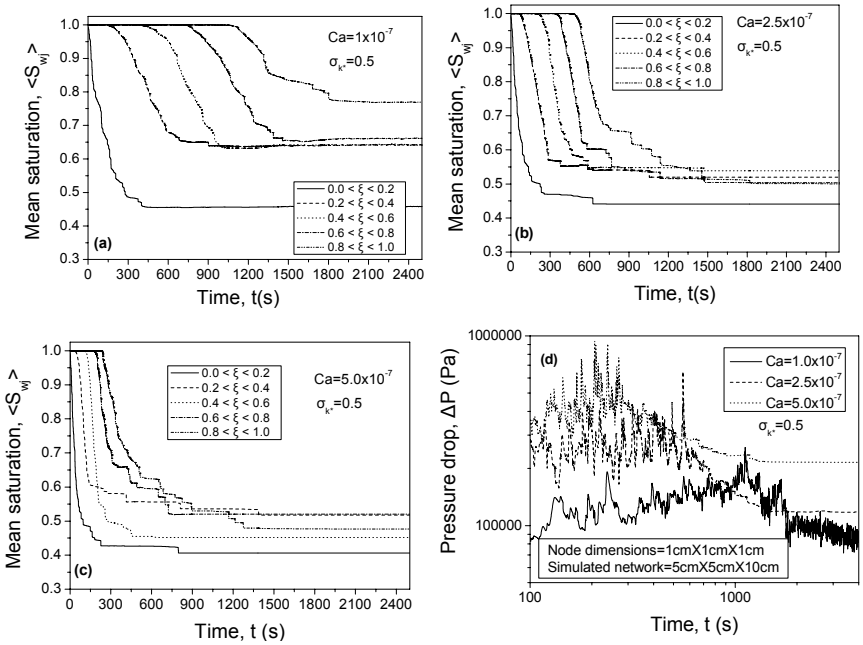

Figure 3. Simulated transient responses of the averaged water saturation profile for capillary number (a) $Ca=1x10^{-7}$, (b) $Ca=2.5x10^{-7}$, (c) $Ca=5x10^{-7}$. (d) Simulated transient response of the pressure drop.

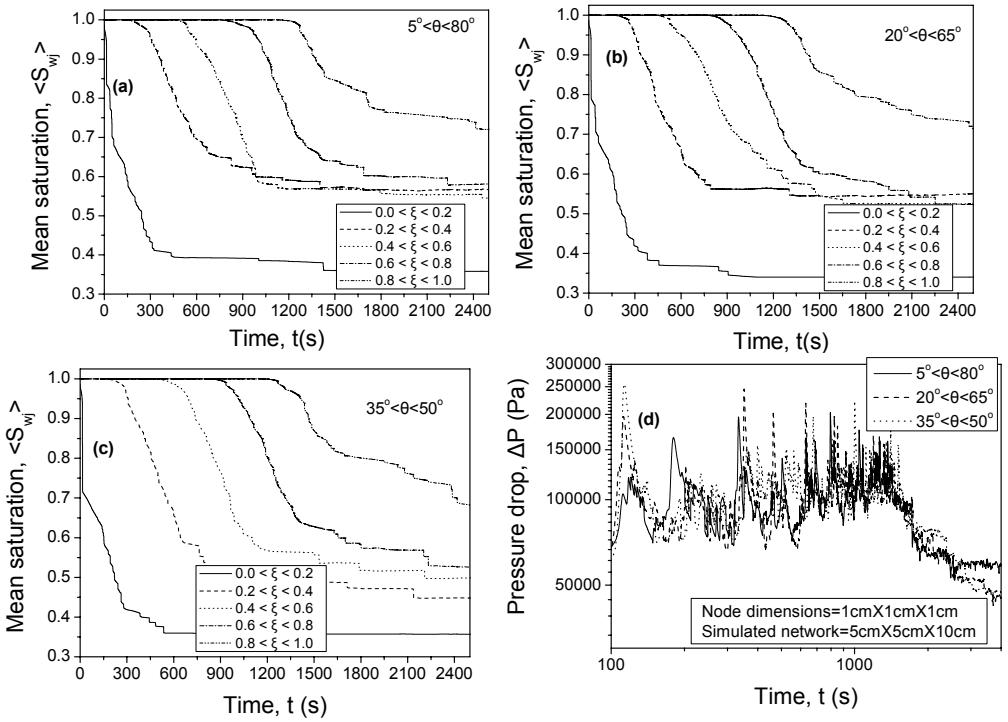

Figure 4. Simulated transient responses of the (a-c) averaged water saturation profile (d) pressure drop for constant permeability (k=50mD) and various widths of the contact angle distribution.

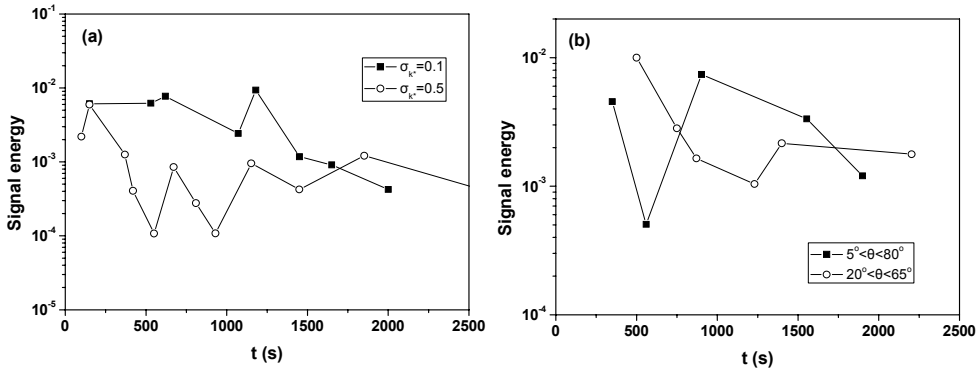

Figure 5. Temporal variation of the wavelet detail (BLCPS) energy for the pressure drop signals obtained with large-scale dynamic simulations on networks of varying (a) permeability distribution, and (b) contact angle distribution.

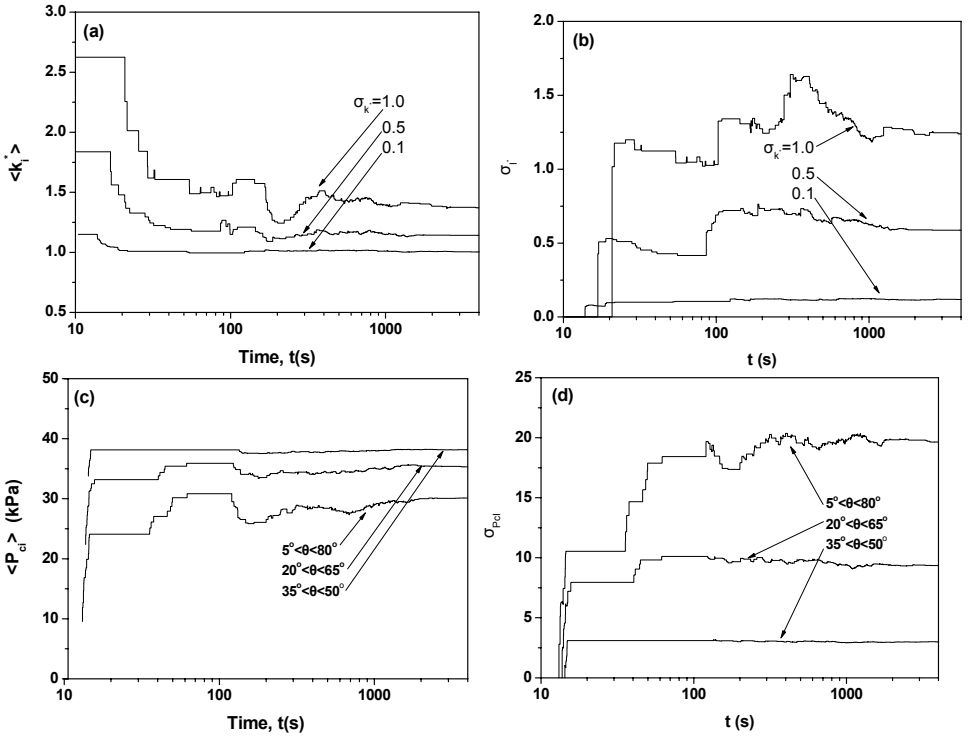

Figure 6. Transient variation of the (a) mean value and (b) standard deviation of the oil-occupied node permeability distribution when the width of the permeability distribution changes. Transient variation of the (c) mean value and (d) standard deviation of the oil-occupied node capillary pressure distribution when the width of the contact angle distribution changes.

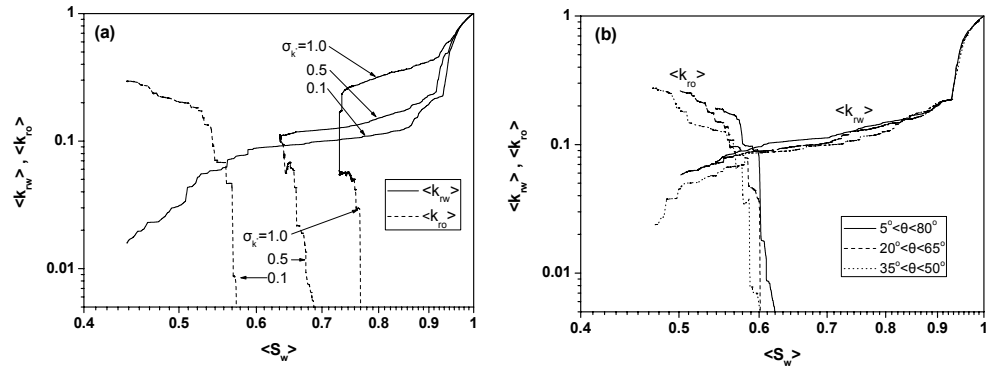

Figure 7. Up-scaled oil and water relative permeability curves obtained with large-scale network simulator for various (a) node permeability distributions, (b) node contact angle distributions.

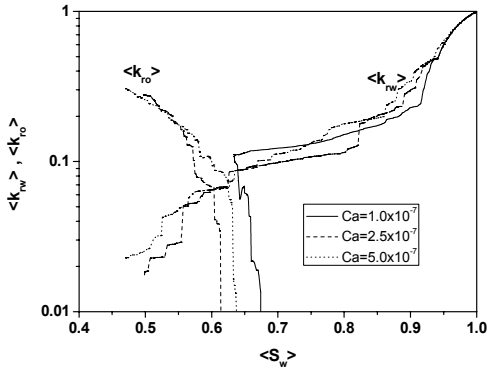

Figure 8. Up-scaled oil and water relative permeability curves obtained with large-scale network simulator for various values of the capillary number.